Rendon-Patiño, A.; Doménech, A.; García Gómez, H.; Primo Arnau, AM. (2019). A reliable procedure for the preparation of graphene-boron nitride superlattices as large area (cm x cm) films on arbitrary substrates or powders (gram scale) and unexpected electrocatalytic properties. Nanoscale. 11(6):2981-2990. https://doi.org/10.1039/c8nr08377k

Reliable Procedure for the Preparation of Graphene-Boron Nitride Superlattice as Large Area (cm×cm) Films on Arbitrary Substrates or Powders (gram scale) and Unexpected Electrocatalytic Properties.

Alejandra Rendón,[a] Antonio Doménech,[b] Hermenegildo García [*a] and Ana Primo [*a]

[a] Instituto de Tecnología Química Consejo Superior de Investigaciones Científicas-Universitat Politècnica de València, Universitat Politecnica de Valencia, Av. De los Naranjos s/n, 46022 Valencia, Spain.

[b] Departamento de Química Analítica, Universitat de Valencia, Av. Del Dr. Moliner 100, Burjassot, Spain

Abstract.

Herein, a reliable procedure for the preparation of graphene-boron nitride superlattice, either as films or powders, consisting in the pyrolysis at 900 ^{o}C of polystyrene embedding pre-formed boron nitride single sheets is reported. The procedure can serve to prepare large area films (cm×cm) of this superlattice on quartz, copper foil and ceramics. Selected area electron diffraction patterns at every location of the films show the occurrence of the graphene-boron nitride superlattice all over the film. The procedure can also be applied to the preparation of powdered samples in gram scale. Comparison with other materials indicates that the superlattice appears spontaneously as the growing

graphene sheets develop, due to the templating effect of pre-existing boron nitride single sheets. Since the characteristic boron nitride emission in the visible region is completely quenched in the superlattice configuration, it is proposed that fluorescence microscopy can be used as a routine technique to determine the occurrence of superlattice in large area films. Electrodes of this material show an unforeseen catalytic activity for oxygen reduction reaction and exhibits a decrease of the heterojunction-electrolyte interphase electrical resistance.

Introduction

Due to its unique electronic, optical and mechanical properties, graphenes are considered as promising materials for a broad range of applications from microelectronics, biomedicine and renewable energies, among others.[1-6] Besides graphene, there is a wide range of related 2D materials having structural analogies with graphene such as boron nitride and molybdenum disulfide.[7-10] These 2D materials are able to form heterojunctions with graphene.[10-12]

It was well-known that the electron mobility and conductive properties of graphene may depend on the substrate, boron nitride being one of the most suitable supports to determine the intrinsic properties of graphene.[13, 14] More recently, it has been shown that the van der Waals assembly of graphene and boron nitride in a configuration in which the hexagons of the two lattices coincide one on top of the other exhibits distinctive properties at the nanoscale as consequence of the modulation of the intrinsic properties of graphene

by the underlying sheet of boron nitride.[15-18] This assembly of graphene and boron nitride with coincident superposition of hexagons has been denoted as *"superlattice"* to remark the matching of the two lattices of the van der Waals G-BN assembly.[19, 20] One field that still remains mostly unexplored is to determine which are the unique properties of the G-BN superlattice different from those of the individual components. Further development of the field and a broad study of the distinctive properties of G-BN superlattices is strongly hampered by the limited availability of this G-BN assembly that occurs in many of the cases reported so far in regions of a few micrometers.[15] Small area G-BN superlattice films can be sufficient to measure physical properties of G-BN superlattice at the nanoscale, confirming theoretical predictions, but they are not sufficiently large for many other practical applications.

Most of the reports on the study of G-BN superlattice describe the preparation of this supramolecular assembly as the random deposition of one material on top of the other.[15, 21, 22] This random deposition of 2D materials is clearly unsatisfactory and only leads to the occurrence of superlattice in small submillimetric areas.

Trying to circumvent this limitation, films of G-BN superlattice from tens of nanometers to millimeters have been obtained by growing graphene on top of boron nitride deposited by photolithography.[23] From the current knowledge it seems that preformed BN can template the epitaxial growth of nascent graphene, but since BN has no dehydrogenation catalytic properties, other techniques different from the conventional chemical vapor deposition of hydrocarbons on metal (Cu and Ni) surfaces are needed. In this regard, epitaxial growth of graphene on boron nitride in superlattice configuration has

also been reported by using plasma assisted decomposition of methane, but the size of the films are limited by the size of boron nitride sheets.[24] There are reports describing epitaxial growth on CVD-formed BN on copper using benzoic acid or by pyrolysis of a sandwiched film of Ni(C)/BN precursor/Ni.[25, 26] Other methods trying to overcome the limitation in the area of the superlattice film have also been reported.[27]

Development of the field of van der Waals graphene-boron nitride superlattice with the exploitation of the new properties and applications that these materials may offer is strongly dependent on the easy availability of this novel material and the description of reliable procedures for the preparation of G-BN superlattices, either as large area (larger than submillimetric scale) films or even in large quantities as a powders that can be dispersed in liquid media.

Herein we disclose a procedure for the preparation of G-BN superlattices as large area (cm×cm) films on arbitrary substrates or as powders in near gram quantities starting from easily available precursors. This method has allowed us to determine the remarkable electrocatalytic properties of the superlattice for the oxygen reduction reaction, one of the key reactions in future emergent technologies to store renewable electricity. This electrocatalytic activity is observed for N-doped graphenes, but it is generally absent in undoped graphenes.[28, 29] However, it seems that the strong van der Waals interaction with underlying BN and modulation of the electronic properties of G in the superlattice is responsible for the observed electrocatalytic activity.

Results and Discussion

The G-BN superlattice preparation procedure is illustrated in Scheme 1. The method derives from the known ability of polystyrene (PS) as additive to exfoliate bulk hexagonal boron nitride crystals (bulk-BN) [30, 31] and the unforeseen ability of PS to form graphene upon pyrolysis at temperatures of around 900 ^{o}C.[32] Thus, upon sonication at ambient temperature, a suspension of bulk-BN in dichloromethane containing PS (M_w 280 000 amu) and removal of the remaining undispersed solid particles, a dispersion of exfoliated BN, mostly as single layer, stabilized by PS is formed. This is in accordance with previous studies on procedures for bulk-BN exfoliation.[31, 33] It is likely that the van der Waals interaction between the aromatic rings of PS and the boron nitride sheet is responsible for the occurrence of the exfoliation of the bulk 3D crystals and dispersion of the BN sheets in the liquid medium.

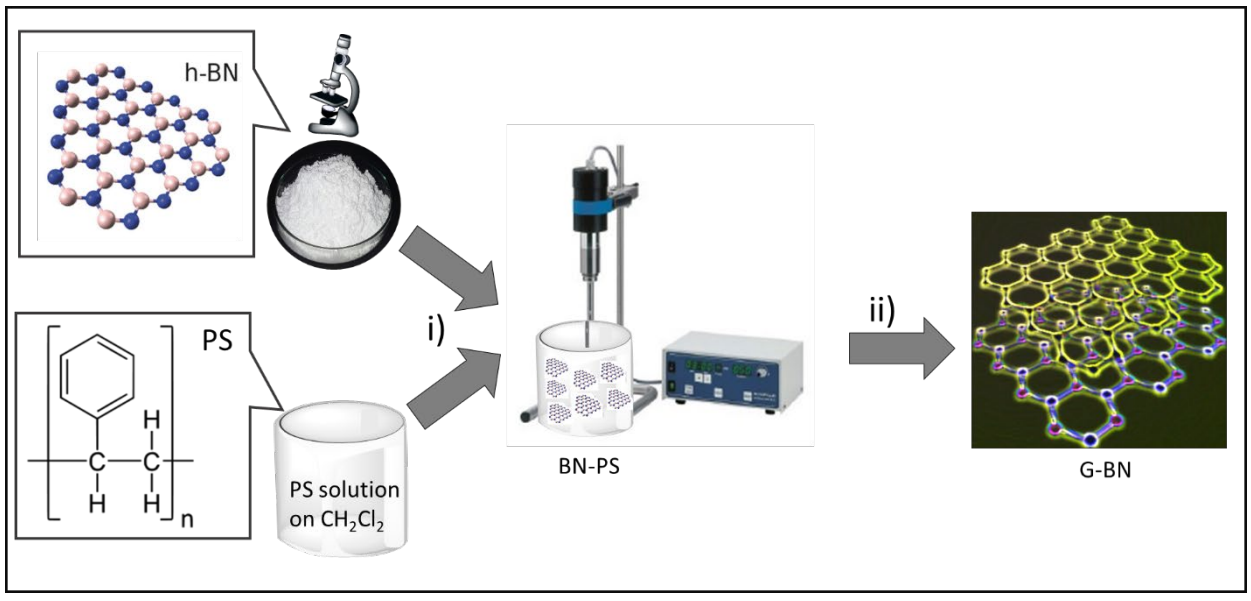

Scheme 1. Illustration of the preparation procedure of G-BN superlattice based on exfoliation of bulk BN crystals by PS in CH_2Cl_2 (i) and subsequent pyrolysis under inert atmosphere of the BN-PS composite (ii).

Characterization of the exfoliated BN suspension in CH_2Cl_2 containing PS by atomic force microscopy (AFM) is compatible with the presence of single or few-layers BN sheets embedded within a polystyrene matrix (Figure 1). The plastic properties of PS makes possible to use this dispersion to form high quality, thin, submicrometric films of exfoliated PS-BN on several substrates, particularly metals, ceramics and glasses. Dichloromethane removal also allows to recover plastic PS embedding exfoliated BN as a thick composite that can be submitting to milling to obtain white powders.

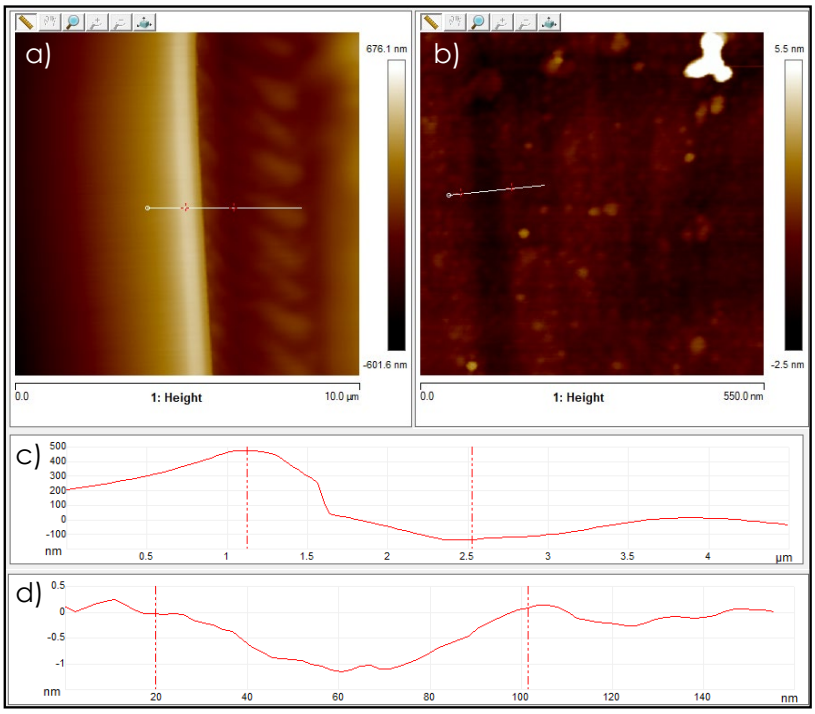

Figure 1. a and c) AFM image of PS-BN composite on quartz where the PS film thickness measured across the white line is about 500 nm and b and d) AFM image of G-BN film resulting from the pyrolysis of PS-BN shown in (a) where the G film thickness measured is about 1 nm corresponding to single layer graphene on top of single layer BN. Note that the white spots observed in panel b correspond to dust since the process was not performed in a clean room.

Preliminary studies showed that pyrolysis of PS, either as films or powders, at temperatures about 900 ^{o}C forms defective graphene as films or dispersions in a liquid after treatment of the powders by ultrasound in these liquids.[32] Supplementary information provides a set of spectroscopic data and images of the materials obtained. Raman spectra of these materials show the presence of the expected 2D, G and D peaks at wavenumbers about 2750, 1590 and 1350 cm^{-1}, respectively. Observation of the D peak is indicative of the presence of structural defects,[34] probably caused by the imperfect condensation of aromatic rings in the final graphene. AFM measurements of films show that pyrolysis has decreased considerably the thickness of the PS precursor film and is consistent with the formation of single or few-layers graphene, depending on the thickness of the PS precursor film (see experimental section). TEM of the suspended material after pyrolysis or upon detachment from the solid substrate also shows the characteristic sheet morphology with light contrast compatible with the formation of single or few-layers graphene. In the case of pyrolysis of thicker polystyrene films, XRD exhibits a pattern with broad diffraction peaks at 23^{o} that indicate the formation in the pyrolysis of graphitic carbon residue with loose packing among the graphene sheets.

In view of the above-results, it could be anticipated that pyrolysis under the same conditions of PS embedding boron nitride sheets will form also similar defective graphene sheet. In accordance with these expectations, when BN-PS precursor films were submitted to pyrolysis under the same conditions previously commented for PS, formation of defective graphene in closer contact with BN sheets was also observed.

AFM images of these G-BN films obtained by pyrolysis of PS-BN (see experimental section) show a flat surface with low rugosity and the presence of some bumps, presumably associated to the quartz substrate. Importantly, the subnanometric vertical resolution of AFM allows to determine the thickness of G-BN films prepared under optimal conditions, measuring a thickness value about 0.7 nm that is compatible with the presence of a single G layer on top of a single BN layer (Figure 1).

Figure 2 shows a comparison of the Raman spectra of defective graphene obtained by PS pyrolysis with that of G-BN superlattice. In the second case, the characteristic narrow Raman peak characteristic of BN appearing at 1365 cm^{-1} overlaps with the broader D band of defective graphene at 1350 cm^{-1}, giving the wrong impression of an increase in the defect densitiy.

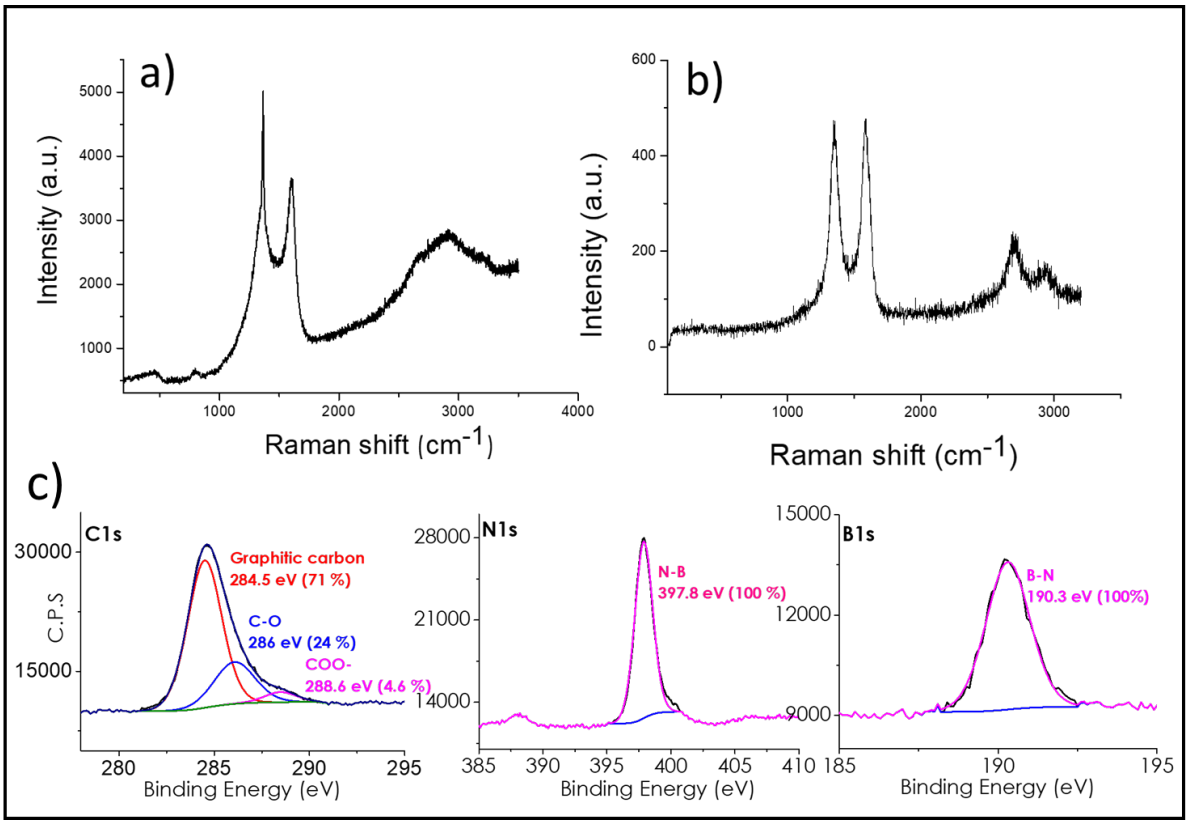

Figure 2. Raman spectra of a) G-BN superlattice and b) defective graphene obtained by PS pyrolysis; note that the sharper line at 1350 cm^{-1} is due to the overlap of the broad graphene D band and the BN sharp peak. c) Deconvoluted XPS C1s, N1s and B1s peaks of G-BN superlattice film on Cu foil. Note that similar XPS peaks are recorded on other substrates, but the C1s peak exhibits a higher proportion of graphitic carbon.

XPS confirms the presence of a sheet of defective graphene on top of BN. Deconvolution of the B1s and N1s shows that they are constituted by almost a single component at binding energy values of 190.3 and 397.8 eV in an atomic proportion 1:1 in good agreement with the earlier reports in the literature for B and N atoms in BN forming G-BN superlattice.[25, 26] The minor components (less than 5 %) observed in the best fitting of

N1s and B1s peaks could be attributed to defects on the BN sheets or to the occurrence Iof some doping on the graphene layer. Deconvolution of the C1s shows predominantly the presence of a component at 284.5 eV corresponding to graphitic carbon. In quartz and ceramics this component was over 90 % in percentage. However, on copper foil, the existence of significant component of C atoms bonded to oxygen atoms of about 24 % was also observed, together with the graphitic C atoms (see Figure 2c).

Scanning electron microscopy of G-BN superlattice films shows a smooth surface without apparent cracks and defects (Figure 3a). Quantitative elemental analysis indicates the presence of B and N in quasi equivalent atomic proportion corresponding to the BN sheets from exfoliation of bulk-BN and lesser C percentage due to the graphene overlayer.

The most relevant information convincingly supporting the superlattice configuration of the two layers was obtained by TEM. While high resolution TEM allows to observe the atomic alignment characteristic of graphene and boron nitride, selected area electron diffraction (SAED) shows the remarkable alignment of G and BN sheets as deduced from the coincidence of the corresponding electron diffraction patterns corresponding to G and B in selected areas. Figure 3 shows also a selected TEM image and the corresponding SAED pattern. Of note is the fact that this characteristic SAED with coincident diffraction peaks for G and BN was recorded at every location monitored in the 1×1 cm^2 films, proving that this superlattice is occurring all over the large area films. The preparation procedure has been repeated numerous times, with reproducible results in terms of the occurrence of large area G-BN superlattice and consistent SAED patterns. Besides quartz, Cu foil and

ceramics were also used as substrate for films, observing in every case the coincidence of the SAED patterns for G and BN sheets.

Pyrolysis of PS-BN powders can also be adapted to the formation of G-BN superlattice as powders by pyrolysis of PS-BN powders obtained by milling the residue after removal of the solvent of the exfoliation step. In the initial pyrolysis steps, the PS-BN composite melts and forms a thick film on the ceramic crucible used in the pyrolysis. After pyrolysis, the carbon residue obtained with the appearance of a thick film was scratched from the ceramic crucible and milled as powder. Sonication of these carbonaceous powders allowed to observe TEM images of the van der Waals G-BN assembly and SAED at every region showing the presence of G-BN superlattice. The specific surface area of the powder was, however, less than 20 $m^2 \times g^{-1}$, indicating the stacking of the layers in the solid material.

Considering the reported results of G-BN superlattice, where formation of graphene by plasma assisted treatment of precursor molecules on BN sheets that have proposed epitaxial growth of graphene on BN,[24, 35] the most reasonable explanation of the superlattice formation under our conditions is the templation effect by the pre-existing BN sheets on the graphene being formed from PS during the pyrolysis process. Templation of nascent graphene by the pre-existing BN sheets has also been claimed in other cases.[25, 26]

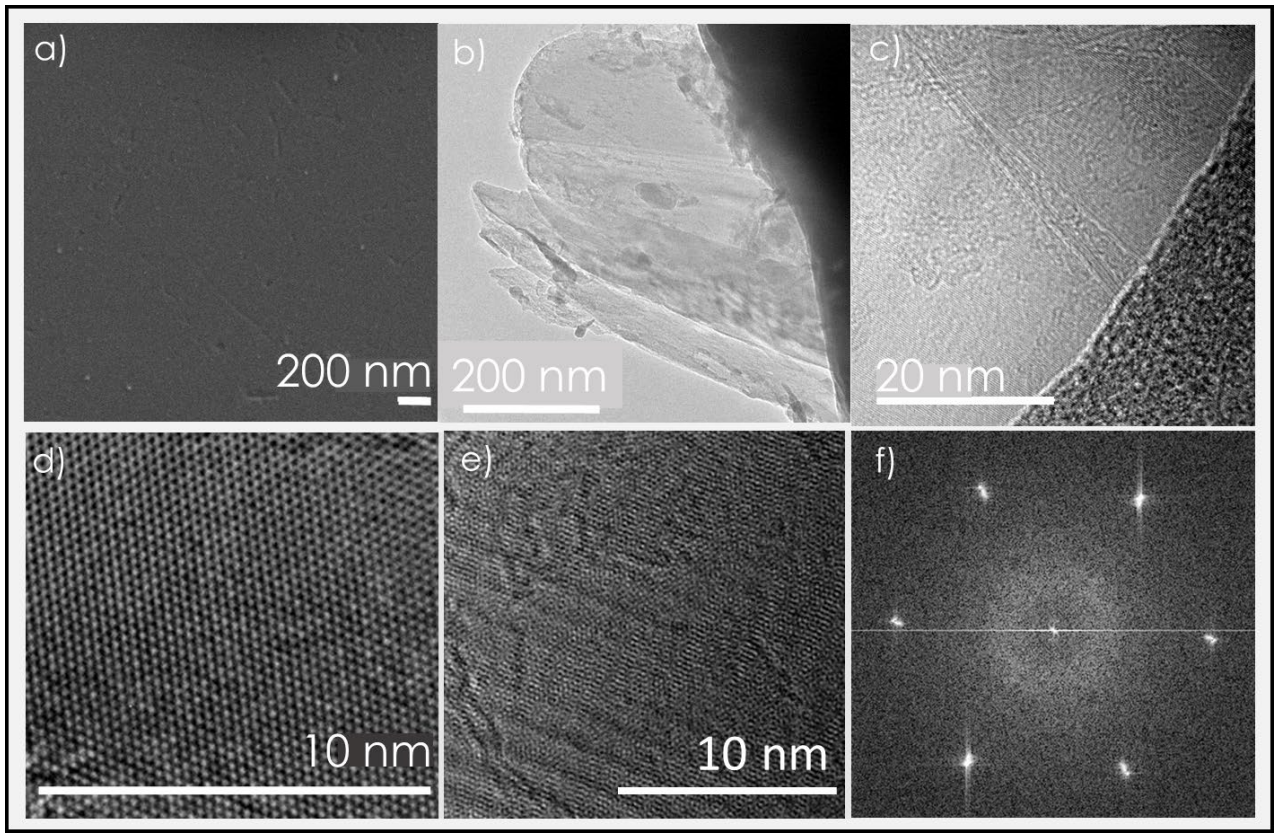

Figure 3. a) Scanning electron microscopy of G-BN superlattice; b), c) Transmission electron microscopy of G-BN superlattice and high resolution TEM of d) h-BN film and e) G-BN superlattice; f) Selected area electron diffraction (SAED) pattern of G-BN superlattice. Note the coincidence of the diffraction points corresponding to G and BN, corresponding to the superlattice configuration.

This explanation is compatible with the superlattice being the thermodynamically more stable configuration of the G-BN assembly due to maximization of the van der Waals interactions and with the conditions of slow formation of G from polystyrene in the pyrolytic process.

To provide some experimental support to the previous proposal and, more specifically to show that graphene sheet formation is a pre-requisite to achieve a superlattice configuration of the G and BN sheets, a commercial sample of G and exfoliated BN sheets were suspended together and submitted to ultrasound mixing before casting a film by spin coating. The G and BN mixture as film was submitted to pyrolysis under the conditions previously used for the formation of the G-BN superlattice. Characterization by TEM and SAED showed that superlattice configuration is not observed at any of the various locations of the film that were monitored. Moreover, a region with the occurrence of G-BN superlattice could never be found in any of the several trials that were carried out. Supplementary information presents some representative TEM images and SAED obtained for these control samples. The failure to observe superlattice is in agreement with the difficulty to achieve this heterojunction configuration by random deposition of the two preformed materials. This shows the importance of graphene growth on BN. Compared to the precedents in the literature, the procedure disclosed here has the advantage that does not require plasma assistance and can be adapted for the preparation of very large areas on arbitrary supports or can serve to prepare powders that can be later suspended in solvents. This shows the uniqueness of the preparation procedure based on the pyrolysis of BN-PS precursors.

It has been recently reported that BN monolayers are bright emitter due to the presence of structural defects.[36-38] We have been able to observe this visible emission in the BN sample obtained by PS exfoliation of bulk-BN. These defects are mainly located at the periphery of the BN sheets, due to the special conditions of these unsatisfactorily

coordinated atoms. Figure 4 shows a representative image of the photoluminescence of these BN-PS films. Furthermore, BN emission is also observed in films of G-BN with a random configuration (Figure 4c), indicating incomplete quenching of the intrinsic BN emission by the inefficient interaction with G.

This bright emission of BN nanosheets obtained by PS exfoliation could also in our case be observed in THF suspensions using a conventional spectrofluorimeter. This allowed us to record their emission spectrum and to establish the possible role of graphene as a quencher of BN emission. Thus, starting from a suspension of BN-PS in THF, addition of increasing amounts of commercial graphene results in a gradual diminution of the emission intensity. Figure 5 shows the typical Stern-Volmer plot confirming the occurrence of BN emission quenching by graphene in suspension. This quenching effect can be understood considering that BN emission derives from the recombination of the charge separated state and that the contact with graphene can lead to electron migration from BN to graphene, decreasing the efficiency of the charge recombination. Therefore, emission intensity should decrease as the concentration of graphene trapping electrons increases, as it was experimentally observed in THF solution.

Importantly, while as commented above the random G-BN assembly does exhibit some residual BN photoluminescence, allowing to record the corresponding image by fluorescence microscopy, the superlattice configuration with over imposition of the G and BN lattices leads to a much more efficient BN emission quenching and, as consequence, the image in fluorescence microscopy of the G-BN superlattice appears black (Figure 4). Figure S7 in supporting information shows a photograph of the G-BN film obtained by pyrolysis of

BN-PS films on quartz. Based on this observation, it is proposed here that optical microscopy is a very simple and straightforward technique to assess the superlattice configuration of large area films of G-BN assemblies. Images by fluorescence microscopy of G-BN heterojunctions in superlattice configuration are black, while those films with random G-BN heterojunctions can be imaged by fluorescence microscopy. Photoluminescence images can be taken with routine equipment, making unnecessary the use of electron microscope to assess the occurrence of superlattice.

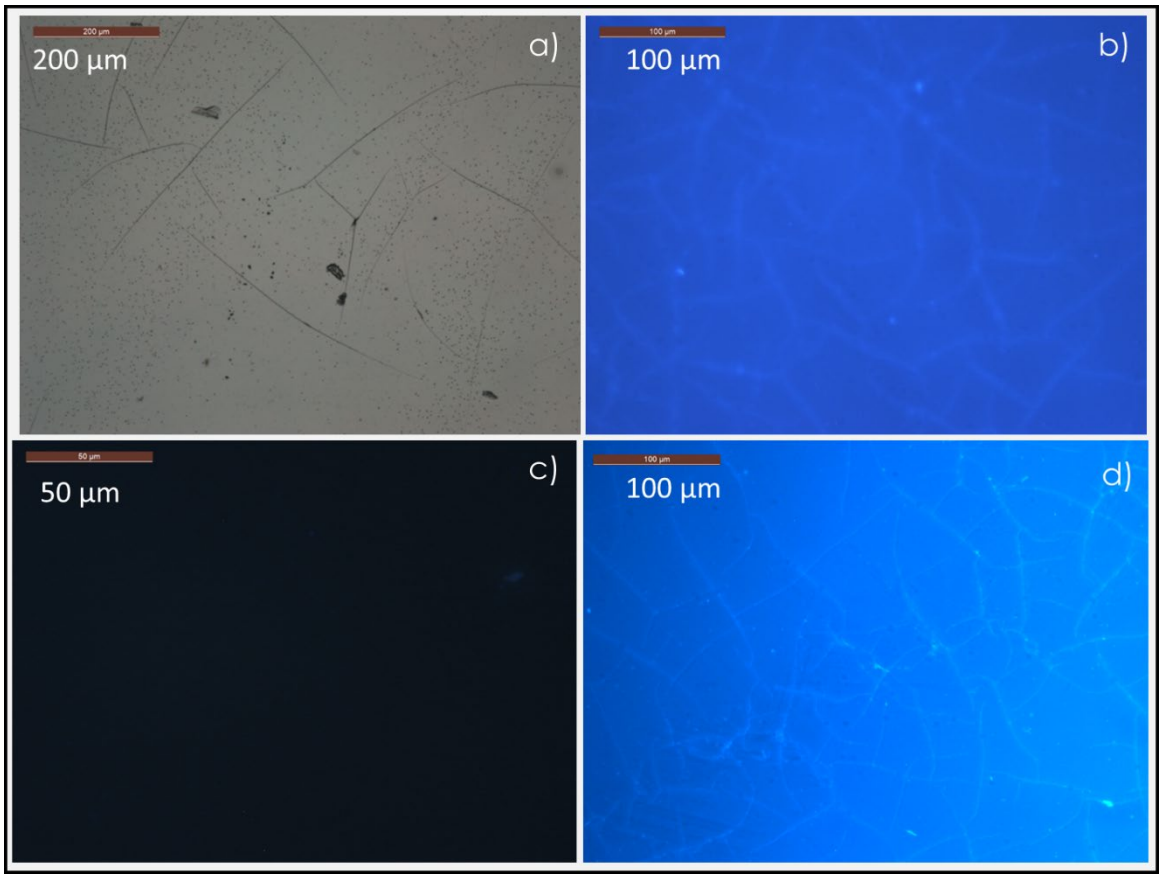

Figure 4. a) Optical and b) fluorescence microscopy images of PS-BN. c) Fluorescence microscopy image of G-BN film in superlattice configuration. d) Fluorescence microscopy image of G-BN film randomly distributed.

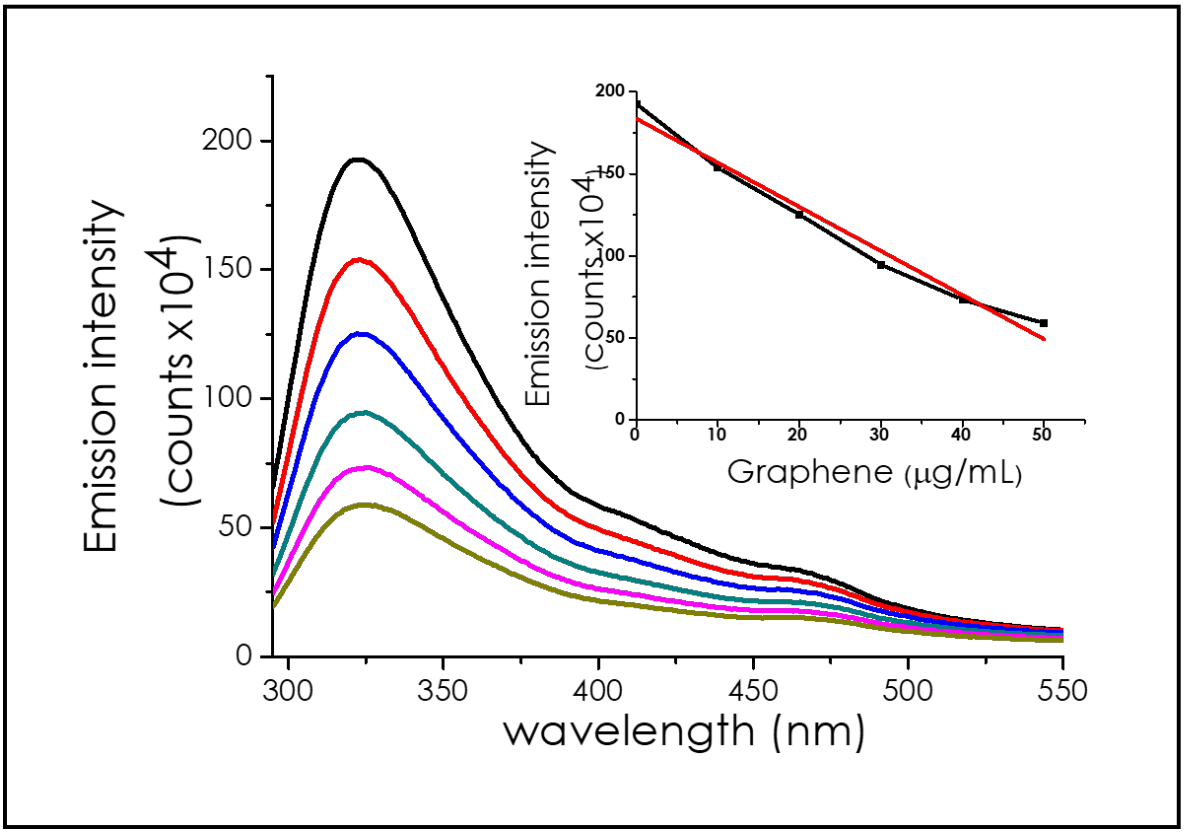

Figure 5. Emission spectra of a BN suspension in THF (1 mg ml) upon excitation at 260 nm and addition of 0 (black), 10 (red), 20 (blue), 30 (green), 40 (magenta) and 50 (dark green) μg ml of G. The inset shows the corresponding Stern-Volmer plot of the emission intensity vs, the concentration of G, confirming the BN emission quenching by graphene.

The availability of large areas of G-BN superlattice films allowed us also to study their electrochemical properties, observing an unforeseen electrocatalytic behavior for the oxygen reduction reaction. Electrocatalysis is one of the areas where graphenes are currently being used as alternative to more expensive noble metals.[39-41] The electrochemical behavior of three electrodes consisting in defective graphene by pyrolysis of PS, the G-BN superlattice and a randomly stacked G-BN assembly were compared. Remarkably differences in the Nyquist plots for the three electrodes when the $Fe(CN)_6^{3-}/Fe(CN)_6^{4-}$ is used as a redox probe as well as when it is applied a bias potential cathodic enough to promote the reduction of dissolved oxygen in air-saturated phosphate buffer solutions (Figure 5a). This electrochemical response consists of a capacitive loop that can be modeled using the equivalent circuit depicted in Figure 5b. On comparing the spectra of the different graphenes, one can see that the G-BN superlattice exhibits a much smaller radius for the low frequency arch, indicating that this electrode has much lower resistance for transferring electrons in the conditions where the oxygen reduction reaction (ORR) occurs as determined by the charge transfer resistance values (see Table S.1 in Supplementary Information). Consistently, cyclic voltammetric experiments in air-saturated phosphate buffer at the film of G-BN superlattice exhibit an enhanced current for the ORR cathodic wave density about three times higher than that of an analogous film of defective graphene or another film of randomly stacked G-BN (Figure 5c). The ORR current at a potential of −0.90 V vs. Ag/AgCl increases by a factor of 4 in the G-BN superlattice as compared to the electrochemical response of the random G-BN assembly and 8 times higher than that of a G films obtained by pyrolysis of PS in the absence of BN. The

electrocatalytic performance (E_{onset} = 0.64 V vs. RHE, $E_{1/2}$ = 0.44 V vs. RHE; Tafel slope 169 mV decade^{-1}; exchange current 0.35 mA cm^{-2}) of the G-BN superlattice electrode, although below of Pt/C commercial catalyst (Pt/C(20 wt.%, J&M corporation; E_{onset} = 0.93 V vs. RHE, $E_{1/2}$ = 0.79 V vs. RHE; Tafel slope 67 mV decade^{-1}; exchange current 2.59 mA cm^{-2}), is comparable to that of other boron-doped graphene catalysts. [42]

These electrochemical tests indicate that the interaction of G with BN in the superlattice facilitates electron transfer with the aqueous electrolyte and maximizes its electronic configuration for transferring electrons to O_2 present in the solution. While modeling and theoretical calculations are needed to understand the origin of these improved electrochemical responses, the data obtained here clearly show the advantages derived from the G-BN superlattice configuration for the use of these materials as electrodes.

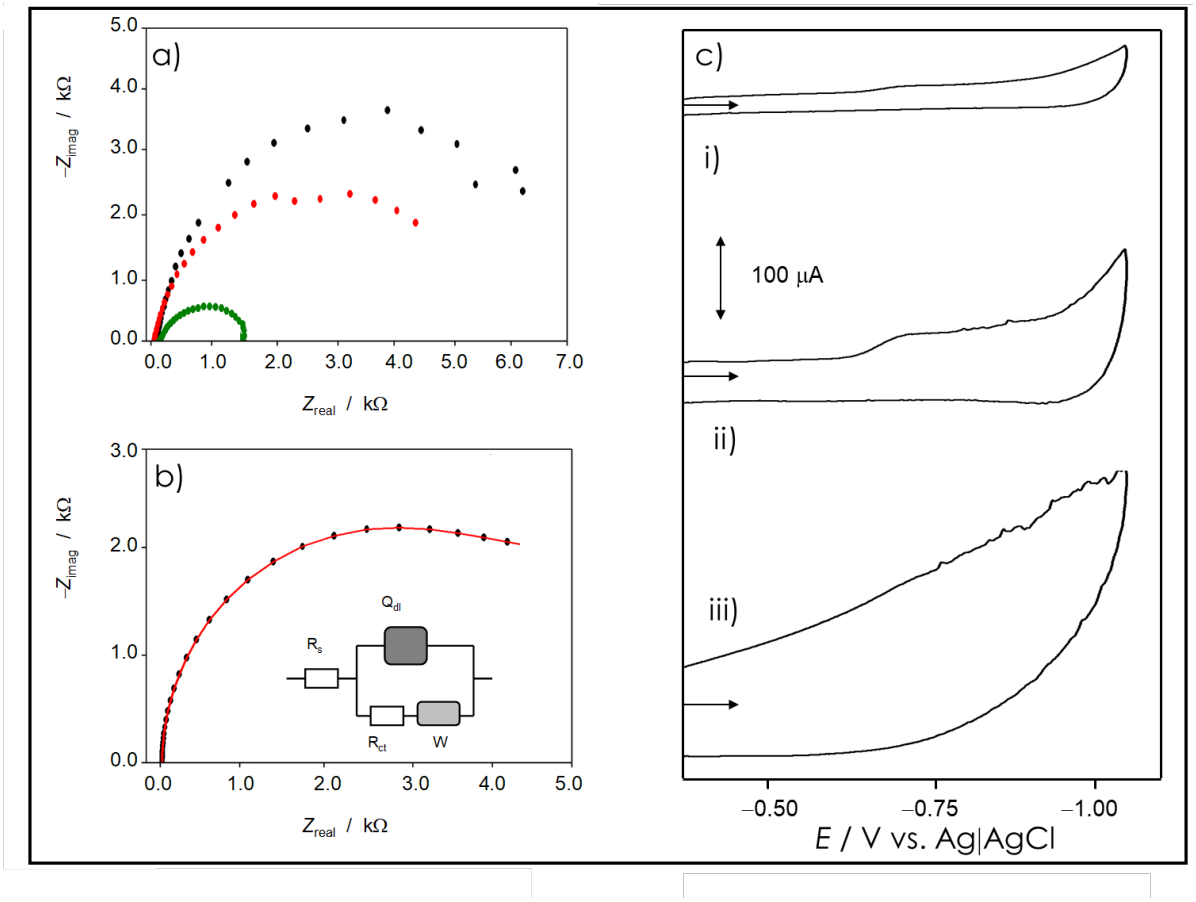

Figure 5. a) Nyquist plots for electrochemical impedance spectroscopy of G from pyrolysis of PS in the absence of BN (black), randomly stacked G-BN assembly (red) and G-BN superlattice (green) sheets in contact with air-saturated 0.10 M potassium phosphate aqueous buffer at pH 7.0; bias potential –0.60 V vs. Ag/AgCl; b) comparison of experimental impedance spectrum for random G-BN assembly with the theoretical model using the equivalent circuit depicted in the inset; c) cyclic voltammograms of i) G from pyrolysis of PS in the absence of BN , ii) randomly stacked G-BN assembly and iii) G-BN superlattice immersed into air-saturated 0.10 M potassium phosphate aqueous buffer at pH 7.0. The arrow indicates the direction of the potential scan; potential scan rate 50 mV s^{-1}.

In summary, the present article has shown a procedure for the preparation of G-BN heterojunction in superlattice configuration as large area films or as powders based on the pyrolysis of exfoliated BN in PS. The procedure appears reliable and appears to derive from the templating effect of BN in the nascent graphene and the higher thermodynamic stability of the superlattice configuration maximizing van der Waals interactions. It is proposed that fluorescence microscopy is a simple and convenient way to assess the occurrence of G-BN superlattice in large area surface. As consequence of the availability of large area films, it has been possible to observe a remarkable enhancement of the electrocatalytic activity of G-BN superlattice for the important electrochemical oxygen reduction reaction.[34-36] This electrocatalytic activity appears to arise from the suitable electron transfer as consequence of the modification of the electronic configuration of G by BN.

Considering the current available information about exfoliation of other 2D materials, it can be predicted that the herein reported procedure can be suitably adapted to prepare other heterojunctions between 2D materials in configurations that maximizes their van der Waals interactions, making available a wide range of these heterojunctions with unforeseen properties. Further work is in progress to prove the general applicability of the present procedure to the preparation of other *superlattice* heterojunctions.

Methods

Exfoliation boron nitride

Commercial boron nitride (Aldrich) at concentration of 1.5 mg/mL was added to a polystyrene (Aldrich) solution of 30 mg/mL in dichloromethane. The mixture was sonicated using a Sonic tip (FisherbrandTM Model 705 at 50% of 700W for 5 hours per sample using 1 s on 1 s off pulsation). After sonication, the dispersion was centrifuged at 1500 rpm for 45 min (Hettich Zentrifugen EBA 21) and the supernatant was collected. To prepare the films, the supernatant was preconcentrated by evaporating the solvent at room temperature and the solid obtained was redissolved in 10 mL.

Preparation of G-BN

Preparation of G-BN films were prepared as reported before.(ref) Briefly, the films were obtained by spin coating onto 2 x 2 cm^2 quartz substrate (APT-POLOS spin-coater: 4000 rpm, 30 s). Other substrates that were used were ceramic and copper foil. The films were pyrolysed under argon atmosphere using the following oven program: annealing at 200 ^{0}C for 2 h and, then, heating at 10 $^0Cmin^{-1}$ up to 900 ^{0}C for 6 h. Thickness of the PS-BN films and the resulting G-BN film were controlled by varying the concentration of PS from 300 to 30 $mL \times ml^{-1}$ and casting the film at 4000 rpm for 30 s. In this way, films of single layer G on BN were obtained by using the most diluted concentration of 30 $mL \times ml^{-1}$ at 4000 rpm.

Physicochemical characterization

Raman spectra were collected with a Horiba Jobin Yvon‑Labram HR UV‑Visible‑NIR (200‑1,600 nm) Raman Microscope Spectrometer, using a laser with the wavelength of 632 nm. The spectra were collected from 10 scans at resolution of 2 cm^{-1}. Optical microscopy images were obtained with a Leica DM4000 that includes a module for fluorescence

characterization, which consists of a mercury lamp and an Avantes AvaSpec-2048 Fiber Optic Spectrometer, which provides a resolution better than 0.5 nm.

SEM images were acquired by using a JEOL JSM 6300 apparatus equipped with X-MAX detector of OXFORD INSTRUMENTS and TEM images were taken on a Philips CM 300 FEG system with an operating voltage of 100 kV. UV-Vis absorption spectra of transparent G-BN films were measured on a Cary 50 spectrophotometer (Varian, Palo Alto, CA, USA) using a quartz cuvette of 3 mL and a 1 cm optical path. Steady-state fluorescence measurements were carried out using a Photon Technology International (PTI, Germany) LPS-220B spectrofluorometer, equipped with a monochromator in the range of 200–700 nm. Excitation wavelength was 270 nm and emission was recorded from 295-550 nm by 1 nm steps with an integration time of 0.1 sec, averaging three measurements. Time-resolved fluorescence measurements were performed with a Easylife X Filter Fluorescence Lifetime Fluorometer (PTI, Canada) using the following parameters: starting time 40 ns, end decay time 250 ns, number of channels 100, integration time 0.1 sec, averaging two measurements at a gain between -1,0 to 1.0 V. Surface area measurement of powders after milling thick residues from PS-BN pyrolysis were measured by isothermal N_2 adsorption using a Micromeritics ASAP 2000 instrument.

Electrocatalytic measurements

Samples consisted of graphene sheets deposited onto 1 cm x 1 cm copper slides. Such laminas acted as working electrode after blocking the uncovered copper surface with silicone paste. Electrochemical measurements were performed in a conventional three-

electrode electrochemical cell completed with a Ag/AgCl (3 M NaCl) reference electrode and a Pt wire auxiliary electrode using a CH 660I potentiostat. Air-saturated 0.10 M potassium phosphate buffer solution at pH=7 was used as a supporting electrolyte optionally incorporating 5 mM $K_3Fe(CN)_6$ plus 5 mM $K_4Fe(CN)_6$. For EIS experiments, a sinusoidal potential modulation of ±5 mV amplitude in the 105 Hz-10−1 Hz was applied, the bias potential being either that of the formal potential of the $Fe(CN)_6^{3-}/Fe(CN)_6^{4-}$ couple (0.24 V vs Ag/AgCl) and that for the reduction of dissolved oxygen (−0.65 V vs Ag/AgCl).

Acknowledgements.

Financial support by the Spanish Ministry of Economy and Competitiveness (Severo Ochoa and CTQ-2015-69653-CO2-R1) is gratefully acknowledged. AR and AP thanks the Spanish Ministry of Economy and Competitiveness for a postgraduate scholarship and a Ramon y Cajal research associate contract, respectively.

Author's contributions.

A.R. performed the preparation and some characterization of the materials. A.D. performed the electrochemical measurements. A.P. supervised the experiments. H.G and A.P. conceived the experiments and write the manuscript through the contribution of all the coauthors. All the co-authors commented on the results and corrected the manuscript.

Notes

A patent on the disclosed preparation procedure has been filed.

References

1. R. M. Frazier, D. T. Daly, R. P. Swatloski, K. W. Hathcock and C. R. South, *Recent Pat. Nanotechnol.*, 2009, **3**, 164.
2. A. K. Geim and K. S. Novoselov, *Nat. Mater.*, 2007, **6**, 183.
3. H. Hirai, H. Tsuchiya, Y. Kamakura, N. Mori and M. Ogawa, *J. Appl. Phys. (Melville, NY, U. S.)*, 2014, **116**, 083703/1.
4. S. Yu, X. Wu, Y. Wang, X. Guo and L. Tong, *Adv. Mater. (Weinheim, Ger.)*, 2017, **29**, n/a.
5. Z. Sun and H. Chang, *ACS nano*, 2014, **8**, 4133.
6. H. Wang, H. Feng and J. Li, *Small*, 2014, **10**, 2165.
7. M. Xu, T. Liang, M. Shi and H. Chen, *Chem. Rev. (Washington, DC, U. S.)*, 2013, **113**, 3766.
8. R. Mas-Balleste, C. Gomez-Navarro, J. Gomez-Herrero and F. Zamora, *Nanoscale*, 2011, **3**, 20.
9. A. Gupta, T. Sakthivel and S. Seal, *Progress in Materials Science*, 2015, **73**, 44.
10. S. Z. Butler, S. M. Hollen, L. Cao, Y. Cui, J. A. Gupta, H. R. Gutiérrez, T. F. Heinz, S. S. Hong, J. Huang and A. F. Ismach, *ACS nano*, 2013, **7**, 2898.
11. K. Novoselov, A. Mishchenko, A. Carvalho and A. C. Neto, *Science*, 2016, **353**, aac9439.
12. D. Jariwala, T. J. Marks and M. C. Hersam, *Nature materials*, 2017, **16**, 170.
13. C. R. Dean, A. F. Young, I. Meric, C. Lee, L. Wang, S. Sorgenfrei, K. Watanabe, T. Taniguchi, P. Kim and K. L. Shepard, *Nature nanotechnology*, 2010, **5**, 722.
14. P. Zomer, M. Guimaraes, N. Tombros and B. Van Wees, *Physical Review B*, 2012, **86**, 161416.
15. M. Yankowitz, J. Xue, D. Cormode, J. D. Sanchez-Yamagishi, K. Watanabe, T. Taniguchi, P. Jarillo-Herrero, P. Jacquod and B. J. LeRoy, *Nature Physics*, 2012, **8**, 382.
16. A. Woessner, M. B. Lundeberg, Y. Gao, A. Principi, P. Alonso-González, M. Carrega, K. Watanabe, T. Taniguchi, G. Vignale and M. Polini, *Nature materials*, 2015, **14**, 421.
17. T. P. Kaloni, Y. Cheng and U. Schwingenschlögl, *Journal of Materials Chemistry*, 2012, **22**, 919.
18. J. Wang, F. Ma and M. Sun, *RSC Adv.*, 2017, **7**, 16801.
19. C.-H. Park, L. Yang, Y.-W. Son, M. L. Cohen and S. G. Louie, *Nature Physics*, 2008, **4**, 213.
20. B. Xu, Y. Lu, Y. Feng and J. Lin, *Journal of Applied Physics*, 2010, **108**, 073711.
21. J. Xue, J. Sanchez-Yamagishi, D. Bulmash, P. Jacquod, A. Deshpande, K. Watanabe, T. Taniguchi, P. Jarillo-Herrero and B. J. LeRoy, *Nature materials*, 2011, **10**, 282.
22. O. Guler and S. H. Guler, *Optik*, 2016, **127**, 4630.
23. Z. Liu, L. Ma, G. Shi, W. Zhou, Y. Gong, S. Lei, X. Yang, J. Zhang, J. Yu, K. P. Hackenberg, A. Babakhani, J.-C. Idrobo, R. Vajtai, J. Lou and P. M. Ajayan, *Nature Nanotechnology*, 2013, **8**, 119.
24. W. Yang, G. Chen, Z. Shi, C.-C. Liu, L. Zhang, G. Xie, M. Cheng, D. Wang, R. Yang, D. Shi, K. Watanabe, T. Taniguchi, Y. Yao, Y. Zhang and G. Zhang, *Nature Materials*, 2013, **12**, 792.
25. T. Gao, X. Song, H. Du, Y. Nie, Y. Chen, Q. Ji, J. Sun, Y. Yang, Y. Zhang and Z. Liu, *Nature communications*, 2015, **6**, 6835.
26. C. Zhang, S. Zhao, C. Jin, A. L. Koh, Y. Zhou, W. Xu, Q. Li, Q. Xiong, H. Peng and Z. Liu, *Nature communications*, 2015, **6**, 6519.

27. A. Woessner, M. B. Lundeberg, Y. Gao, A. Principi, P. Alonso-González, M. Carrega, K. Watanabe, T. Taniguchi, G. Vignale, M. Polini, J. Hone, R. Hillenbrand and F. H. L. Koppens, *Nature Materials*, 2014, **14**, 421.
28. L. Qu, Y. Liu, J.-B. Baek and L. Dai, *ACS nano*, 2010, **4**, 1321.
29. L. Lai, J. R. Potts, D. Zhan, L. Wang, C. K. Poh, C. Tang, H. Gong, Z. Shen, J. Lin and R. S. Ruoff, *Ener. Environ. Sci.*, 2012, **5**, 7936.
30. V. Nicolosi, M. Chhowalla, M. G. Kanatzidis, M. S. Strano and J. N. Coleman, *Science*, 2013, **340**.
31. P. May, U. Khan, J. M. Hughes and J. N. Coleman, *The Journal of Physical Chemistry C*, 2012, **116**, 11393.
32. A. Rendon, A. Domenech, H. garcia and A. Primo, submitted for publication.
33. U. Khan, P. May, A. O'Neill, A. P. Bell, E. Boussac, A. Martin, J. Semple and J. N. Coleman, *Nanoscale*, 2013, **5**, 581.
34. J.-B. Wu, M.-L. Lin, X. Cong, H.-N. Liu and P.-H. Tan, *Chem. Soc. Rev.*, 2018, **47**, 1822.
35. N. Mishra, V. Miseikis, D. Convertino, M. Gemmi, V. Piazza and C. Coletti, *Carbon*, 2016, **96**, 497.
36. T. T. Tran, K. Bray, M. J. Ford, M. Toth and I. Aharonovich, *Nature nanotechnology*, 2016, **11**, 37.
37. G. Grosso, H. Moon, B. Lienhard, S. Ali, D. K. Efetov, M. M. Furchi, P. Jarillo-Herrero, M. J. Ford, I. Aharonovich and D. Englund, *Nature communications*, 2017, **8**, 705.
38. N. Chejanovsky, M. Rezai, F. Paolucci, Y. Kim, T. Rendler, W. Rouabeh, F. Fávaro de Oliveira, P. Herlinger, A. Denisenko and S. Yang, *Nano letters*, 2016, **16**, 7037.
39. C. Zhu and S. Dong, *Nanoscale*, 2013, **5**, 1753.
40. J. Duan, S. Chen, M. Jaroniec and S. Z. Qiao, *ACS Catalysis*, 2015, **5**, 5207.
41. B. Xia, Y. Yan, X. Wang and X. W. D. Lou, *Materials Horizons*, 2014, **1**, 379.
42. L. Qin, L. Wang, X. Yang, R. Ding, Z. Zheng, X. Chen and B. Lv, *J. Catal.*, 2018, **359**, 242.